

The Effect of Phosphorus Content on the Structure and Wear Properties of Electrodeposited Nanocrystalline Ni-P Alloys

*D.H. Jeong, U. Erb, K.T. Aust and G. Palumbo**

Dept. of Materials Science and Engineering, University of Toronto, Toronto, Canada

**Integran Technologies Inc., Toronto, Canada*

The structure and wear properties of nanocrystalline Ni-P electrodeposits have been studied using X-ray diffraction, electron microscopy and Taber wear testing. It is shown that the wear properties change significantly in the range of 0.5~5.9 wt% P. Wear resistance was found to be the highest in Ni-1.8 wt% P electrodeposits. This composition showed the maximum hardness in this series of materials and corresponded to the critical grain size (~9 nm) at which a transition from regular to inverse Hall-Petch behavior was observed. Coatings with average grain sizes smaller or larger than this grain size (i.e. with P content higher or lower than 1.8 wt%) showed lower hardness and thus reduced wear resistance.

For more information, contact:

D.H. Jeong, c/o Prof. U. Erb
Dept. of Materials Science and Eng.
University of Toronto
Toronto, Ontario
Canada, M5S 3E4

1. Introduction

Hard surface coatings are frequently used to improve the resistance to wear, especially abrasive wear, of engineering components. Nickel phosphorus (NiP) alloys are of great importance because of their excellent performance as wear resistant coatings, which also provide very good corrosion protection^{1,2}.

Since the first development of the electrodeposition process for NiP plating by Brenner et al.³ in order to overcome some of the technical drawbacks of the electroless process for NiP plating, such as expensive reducing agents, high operating bath temperature and very sensitive bath chemistry control⁴, electrodeposited NiP coatings have been extensively studied due to several other advantages over the electroless process. These include rapid plating rates, high current efficiency, deposition of very thick coatings, low unit costs and simple equipment requirements⁵⁻⁸.

The wear resistance of NiP coatings can be improved significantly by heat treatment, usually as a result of a phase transformation from amorphous in the as-plated state to a two-phase nickel-nickel phosphide structure after annealing^{1,7}. However, a careful selection of heat treatment conditions is required because annealing can influence the mechanical properties of the substrate material. Traditionally, surface protective coatings of NiP alloys have been extensively used on steel surfaces. In recent years, however, there has also been a rapidly growing interest to apply these coatings on light metals such as aluminum, magnesium and their alloys used for weight reduction of engineering components in the automotive and aerospace industries. Therefore it is of considerable interest to develop wear resistant NiP coatings without the need of post-plating heat treatments to avoid the deterioration of substrate materials.

More recently developed low phosphorus electroless NiP (LPEN) coatings with less than 5~6 wt% P offer superior hardness, excellent wear resistance, good solderability, low electrical resistivity and good corrosion resistance in hot-alkaline environments in the as-deposited state⁹⁻¹⁴. These coatings can meet many critical property requirements. However, plating rates for LPEN are lower than those for both electroless NiP coatings with high phosphorus content and electrodeposited NiP coatings, which is a considerable drawback for commercial usage of this coating system¹⁵.

In the past few years, special attention has been given to the development of nanocrystalline NiP coatings with low phosphorus content produced by the electrodeposition process as a result of their attractive mechanical properties in the as-plated state and high current efficiencies^{5,6}. A number of studies on electrodeposited nanocrystalline NiP coatings have been concerned with microstructural evolution^{5,6}, mechanical properties¹⁶ (e.g. Young's modulus, strength, elongation, fracture), thermal stability¹⁷⁻²⁰, corrosion resistance²¹ and magnetic properties²². However, no studies have been carried out to date to investigate the wear behavior of electrodeposited nanocrystalline NiP coatings with low phosphorus content.

In this study, nanocrystalline NiP coatings with 0.5~5.9 wt% P were produced by electrodeposition and characterized using scanning electron microscopy (SEM), transmission electron microscopy (TEM), X-ray diffraction (XRD) and energy dispersive X-ray spectroscopy (EDS). The effect of the phosphorus content on microstructure, texture, grain size and hardness was evaluated. The influence of these factors on the abrasive wear properties was then assessed using Taber wear testing.

2. Experimental Procedure

The substrates used in this study were AISI 1010 low carbon mild steel with a thickness of ~900 μm and a size of 10 x 10 cm^2 . They were ground using SiC abrasive paper up to 600 grit size, ultrasonically cleaned in acetone for 5 min. and then rinsed using de-ionized water. NiP coatings with low phosphorus content

(LP-NiP) were electroplated onto the substrate from a bath containing nickel sulphate (137 g/l), nickel carbonate (36.5 g/l), phosphorous acid (2~3 g/l), saccharin (5 g/l) and sodium laurel sulphate (0.1 g/l), as described elsewhere²³. Phosphoric acid (H₃PO₄) was used to adjust the pH of the bath solution to pH 1.5; H₃PO₄ not affecting the P content of NiP coatings⁴. The temperature of the bath was maintained at 70 °C and the solution was continuously stirred using a magnetic stirrer. The current density during electrodeposition was 10~30 mA/cm². Bath current density and phosphorous acid concentration were adjusted to produce NiP alloys with P content up to about 6 wt%. Pure nickel (Falconbridge crowns) was used as the anode material. The thickness of the NiP coatings was in the range of 50~80 μm.

The microstructures of NiP coatings were characterized using TEM, SEM, XRD and EDS. For TEM analysis, the Ni-P coatings were thinned to electron transparency by jet polishing using a solution of 75% acetic acid, 15% methanol and 10% perchloric acid at a temperature of -15 °C and an applied voltage of 30 V DC. The average phosphorus content of NiP coatings was determined using SEM/EDS analyses from at least 5 different locations. XRD using Co-Kα (λ=1.7903 Å) radiation was performed for texture evolution and grain size analysis. The peak broadening of the {111} peak at half maximum was used for grain size calculations using Scherrer's formula²⁴,

$$d = \frac{0.9 \cdot \lambda}{B \cdot \cos \theta} \quad (1)$$

where d is the grain size; λ is the wavelength of the Co-Kα radiation; B is the {111} peak broadening; and θ is the Bragg angle of the {111} peak. In addition, TEM dark field images were used to determine the grain size directly by counting more than 250 grain diameters per sample.

The hardness of NiP coatings was measured using a Shimadzu HMV-2000 Vickers microhardness tester with a load of 100g applied for 15 sec. The hardness values reported here are average values of at least five measurements for each coating.

The abrasive wear resistance of the nanocrystalline NiP coatings was assessed using a Taber wear tester; Taber wear testing being one of the most widely accepted methods for evaluating the wear resistance of abrasion-resistant coatings^{7,25,26}. Wear data are expressed by the Taber Wear Index (TWI), which is the weight loss in mg per one thousand cycles of abrasive wear.

$$TWI = \frac{W_b - W_a}{N} \times 1000 \quad (2)$$

where W_a and W_b are the specimen weights in mg after and before the test, respectively, and N is the number of total cycles (here, 10,000 cycles). Table 1 shows the test conditions of the Taber wear test applied in the current study.

Table 1 Test conditions for Taber wear tests used in this study

Abrasive wheel	: CS-17	RPM of turntable	: 90 ± 3
Number of cycles	: 10,000	Temperature	: 23 ± 2 °C
Applied load	: 1,000 g	Humidity	: 50 ± 5 %
* Dry and unlubricated test			
* Wear debris continuously removed by vacuum apparatus			

3. Results and Discussion

3.1. Microstructural evolution

Several representative XRD patterns of the as-plated LP-NiP coatings are shown in Fig. 1, together with the diffraction pattern of a pure polycrystalline Ni (90 μm grain size) with random crystallographic orientation for comparison. As can be seen in this figure, increasing P content resulted in two major changes in the diffraction patterns compared with conventional Ni. First, increasing P content in the deposits led to considerable line broadening. Coatings with P content up to 2.5 wt% showed diffraction patterns typically observed for nanocrystalline materials^{5,6,16,22,20} with well defined, but increasingly broader {111}, {200}, {220}, {311} and {222} diffraction peaks. Using the Scherrer's formula, the grain size in the materials was calculated to decrease from 12.5 nm at 0.5 wt% P to about 8.5 nm at 2.5 wt% P, respectively (see Table 2).

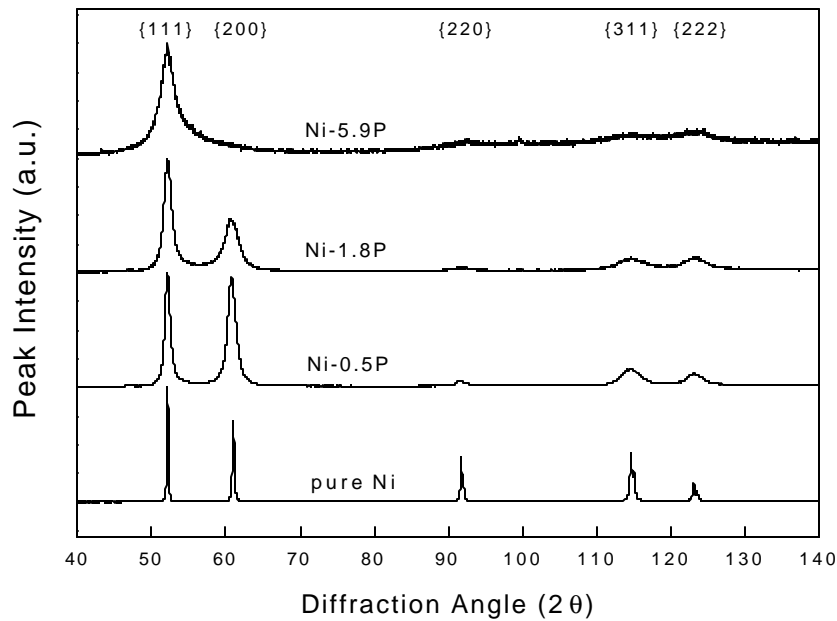


Fig. 1 X-ray diffraction patterns for various NiP coatings and pure polycrystalline Ni standard material

Table 2 Phosphorus content, grain size (as determined by XRD and TEM), texture, hardness and Taber Wear Index of the coatings produced in this study

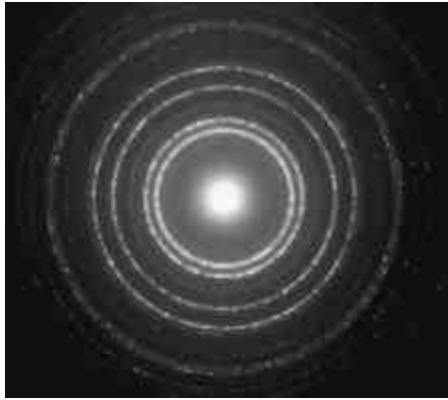
<i>P</i> (wt%)	<i>d</i> -XRD (nm)	<i>d</i> -TEM (nm)	Strongest XRD peaks	Hardness (VHN)	TWI
0.5 ± 0.1	12.5	12.7	{111} {200}	651 ± 17	23.4 ± 1.3
1.2 ± 0.2	10.0	9.4	{111} {200}	691 ± 12	17.2 ± 0.0
1.8 ± 0.2	9.2	8.8	{111} {200}	705 ± 22	16.8 ± 0.2
2.5 ± 0.1	8.5	6.1	{111} {200}	686 ± 22	19.3 ± 1.0
3.4 ± 0.3	(7.3)	*	{111}	635 ± 27	24.8 ± 1.3
5.9 ± 0.3	(4.7)	*	{111}	611 ± 6	26.2 ± 1.5

(*: mixed amorphous/nanocrystalline)

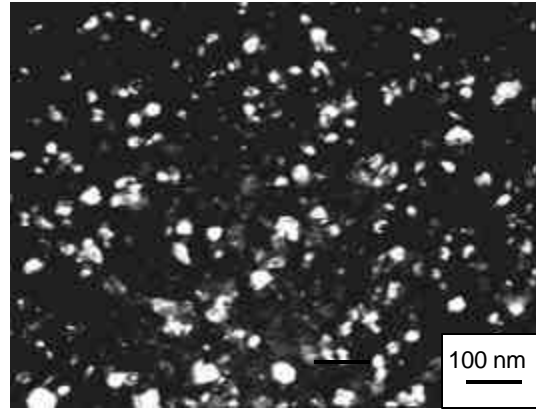
For deposits with 3.4 wt% P and 5.9 wt% P, the diffraction peaks continued to broaden and the patterns showed the characteristic features of the mixed amorphous-nanocrystalline structure or an amorphous structure. Essentially only the {111} diffraction peak remains, similar to what has been previously observed^{5,6}. Even though a grain size is meaningless for the amorphous structure, line broadening was nevertheless used to calculate an apparent grain size of 7.3 nm and 4.7 nm for the deposits containing 3.4 wt% P and 5.9 wt% P, respectively, listed in brackets in Table 2. No additional diffraction peaks for any of the thermodynamically possible^{27,28} Ni-P intermediate phases (e.g. Ni₃P, Ni₅P₂, NiP, etc.) were observed in the as-plated materials. Consequently, these coatings can be considered supersaturated solid solutions of P in nanocrystalline FCC Ni, which approach the amorphous structure at the highest P concentrations.

The second major change in the diffraction patterns with increasing P content is the development of strong crystallographic texture, as can be estimated from the relative peak intensities (see Fig. 1 and Table 2 for strongest XRD peaks). The relative peak intensities for polycrystalline Ni with random crystallographic texture can be derived from the XRD pattern of pure Ni in Fig. 1. For the coatings containing 0.5 wt% P the two strongest peaks are the {111} and {200}, while the intensities of the {220} and {311} peaks have decreased considerably. In other words, the material has a double fiber texture such that the crystals are preferentially aligned with either their {111} or {200} planes parallel to the substrate surface. Further increases in the P content resulted in a decrease in the {200} intensity relative to the {111}, which means that more crystals become preferentially aligned with their {111} planes parallel to the substrate surface. The development of the {111} texture with increasing P content is consistent with the textural evolution previously observed in other studies both in electrodeposited NiP coatings^{1,2,29} and in electroless NiP coatings^{15,30}.

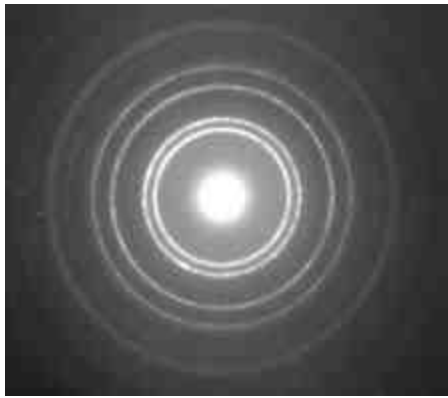
Fig. 2 shows the TEM diffraction patterns and dark or bright field micrographs of some of the as-plated LP-NiP coatings. TEM diffraction patterns of LP-NiP coatings with less than 2.5 wt% P (Figs. 2a, 2c) show well-defined continuous diffraction rings (i.e. {111}, {200}, {220}, {311}, {222}, etc.), which are characteristic of the nanocrystalline structure. The TEM dark field micrographs in Figs. 2b and 2d show the corresponding microstructures for coatings containing 0.5 and 1.8 wt% P, respectively. The structures show equiaxed grains with relatively narrow grain size distributions. By measuring the grain diameter of at least 250 grains on dark field micrographs for each material, the average grain sizes as per TEM analysis shown in Table 2 were obtained for the various LP-NiP coatings produced in this study. It should be noted that these values are in good agreement with the grain sizes determined by XRD.



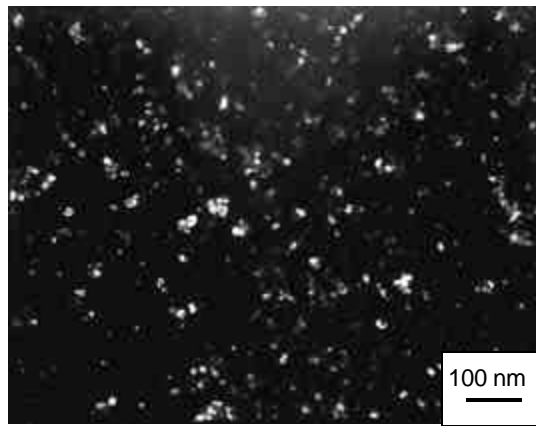
(a) Ni-0.5 wt% P



(b) Ni-0.5 wt% P (Dark field)



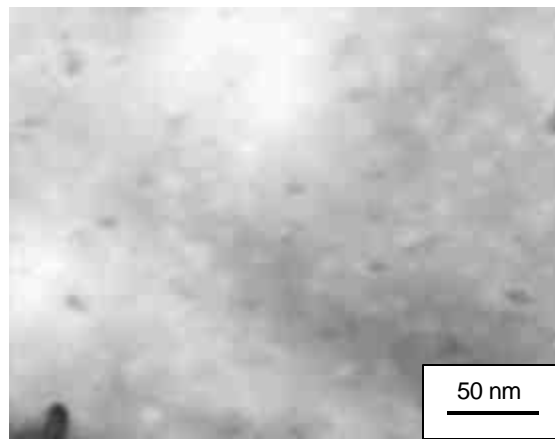
(c) Ni-1.8 wt% P



(d) Ni-1.8 wt% P (Dark field)



(e) Ni-5.9 wt% P



(f) Ni-5.9 wt% P (Bright field)

Fig. 2 TEM diffraction patterns and dark & bright field images of NiP coatings

The diffraction rings begin to show considerable broadening and development of a broad halo for deposits containing 3.4 wt% P. This is due to the formation of an amorphous phase, as suggested in the XRD patterns. An example is shown for the Ni-5.9P coating in Fig. 2e. The corresponding TEM bright field image of Ni-5.9P (Fig. 2f) shows the characteristic microstructure of an amorphous phase, embedded into which several grains with an average size of about 8 nm can be observed. There was no evidence in the TEM diffraction patterns for nickel phosphide formation in any of the as-plated LP-NiP coatings in good agreement with the XRD results.

Based on the findings from the X-ray diffraction scans and electron microscopy, the microstructural evolution in the coatings can be summarized as follows. Increasing P content resulted in, first, considerable grain refinement of supersaturated NiP nanocrystals, second, the development of strong crystallographic orientation and, third, the formation of a mixed amorphous-nanocrystalline structure.

3.2. Hardness and Wear Resistance

Fig. 3 shows the hardness of the LP-NiP coatings as a function of wt% phosphorus. Initially the hardness increases with increasing P content up to 1.8 wt %. This could be due to a solid solution hardening mechanism. However, the subsequent decrease in hardness for coatings with P contents higher than 1.8 wt% is difficult to understand in terms of solute effects. When the hardness values are plotted as a function of $d^{-1/2}$ (where d is the grain size of the material taken from the XRD results shown in Table 2), i.e. in the form of Hall-Petch plot (Fig. 4), a hardness curve similar to the ones found for numerous other nanocrystalline materials is observed^{5,6,31-34}. The initial increase in hardness of these materials can be explained in terms of regular Hall-Petch strengthening^{35,36}, in which the strength/hardness increases with the reciprocal square root of the grain size; this being the result of increasing dislocation/grain boundary interactions when reducing the grain size of the material. On the other hand, for grain sizes less than a critical value, which is dependent upon the material, the inverse Hall-Petch effect is observed^{5,6,31}. While the details of the mechanisms leading to this unexpected softening phenomenon are still not fully

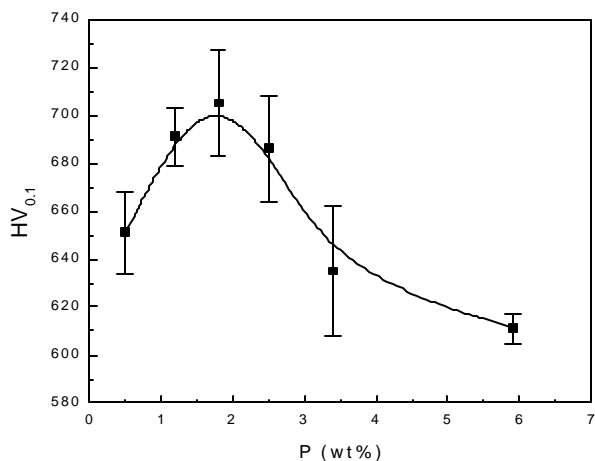


Fig. 3 Hardness as a function of P content

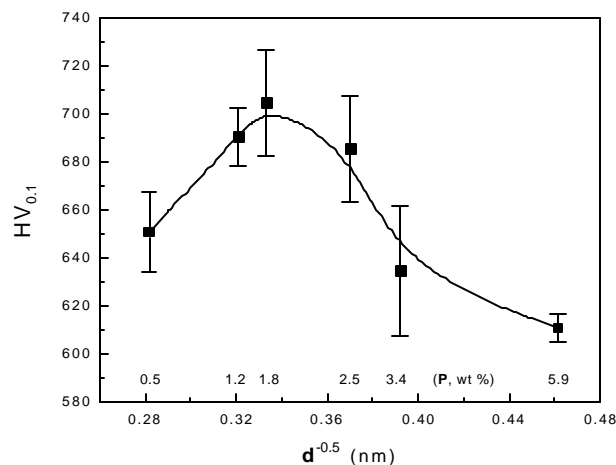


Fig. 4 Hardness as a function of grain size (Hall-Petch plot)

understood, most of the interpretations for this effect are based on a transition from dislocation-controlled deformation to other deformation mechanisms^{5,6,31,32,37,38}, which become dominant at very small grain sizes. It should be noted that the two points of the mixed amorphous-nanocrystalline coatings with 3.4 wt% P and 5.9 wt% P coatings are included in this graph (based on their apparent grain size as determined by XRD, Table 2) to demonstrate the smooth and continuous transition in hardness as the material gradually changes from nanocrystalline to amorphous. This effect has been previously discussed in more detail³².

Fig. 5 shows the Taber wear index (TWI) as a function of the P content. As the P content increases from 0.5 wt% to 1.8 wt%, TWI drops (i.e. wear resistance increases). With further increases in P content, the TWI increases again (i.e. wear resistance decreases). Therefore for these coatings, there is a direct relationship between hardness and TWI (or wear resistance) as expected from Archard's law³⁹. The NiP coating with 1.8 wt% P showed the highest hardness and, consequently, the highest wear resistance.

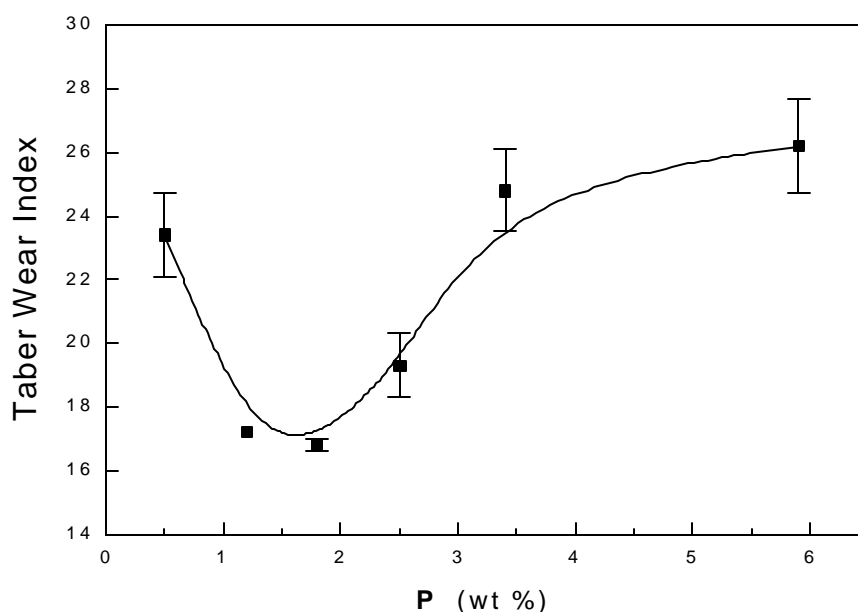


Fig. 5 Taber wear index as a function of P content in the deposits

4. Conclusions

The effect of the P content on microstructure, texture and hardness was evaluated for electrodeposited nanocrystalline NiP coatings with low phosphorus content up to 5.9 wt%, and the influence of these factors on the wear resistance was assessed using Taber wear testing. NiP coatings with P content up to 2.5 wt% were found to be supersaturated solid solutions of P in nanocrystalline Ni. For higher P content, mixed structures of nanocrystalline NiP crystals embedded in an amorphous matrix were obtained. When the hardness is plotted in the form of a Hall-Petch curve, a transition from regular to inverse Hall-Petch behavior is observed. The hardness showed a maximum at 1.8 wt% P which corresponded to a grain size of about 9 nm, and for which the highest wear resistance was observed. The wear resistance was found to be directly related to the hardness, following Archard's law.

Acknowledgments

The authors would like to thank Drs. J. McCrea and G. Hibbard (Integran Technologies Inc.) for their contributions. Financial support from the Natural Sciences and Engineering Research Council of Canada (NSERC) and Ontario Power Generation is gratefully acknowledged. One of the authors (D.H.J.) is supported by an Ontario Graduate Scholarship in Science and Technology (OGSST).

References

1. Lewis, D.B. and Marshall, G.W., *Surf. Coat. Tech.*, **78**, 150 (1996)
2. Ng, P.K., Snyder, D.D. and Lasala, J., *J. Electrochem. Soc.* **135(6)**, 1376 (1988)
3. Brenner, A., Couch, D.E. and Williams, E.K., *J. Res. Nat. Bur. Stand.* **44**, 109 (1950)
4. Narayan, R. and Mungolf, M.N., *Surf. Tech.* **24**, 233 (1985)
5. McMahon, G. and Erb, U., *J. Mat. Sci. Lett.*, **8**, 865 (1989)
6. McMahon, G. and Erb, U., *Microstructural Science*, **17**, 447 (1989)
7. Gawne, D.T. and Ma, U., *Wear*, **129**, 123 (1989)
8. Luke, D.A., *Trans. IMF*, **64(3)**, 99 (1986)
9. Li, J., Hu, X. and Wang, D., *Plat. Surf. Finish.*, **83(8)**, 62 (1996)
10. Jackson, B., Macary, R. and Shawhan, G., *Trans. IMF*, **68(3)**, 75 (1990)
11. Dunkin, B. and Crotty, D., *Proc. AESF SUR/FIN '92*, Atlanta, Georgia, USA. P, 1151, 1992
12. Bayes, M., Sinitskayu, I., Schell, K. and House, R., *Trans. IMF*, **69**, 140 (1991)
13. Bleeks, T. and Shawhan, G., *Met. Finish.*, **87**, 21 (1989)
14. Kreye, H. and Gutmann, R., *Metalloberflache*, **47**, 387 (1993)
15. Zhang, Y.Z. and Yao, M., *Trans. IMF*, **77(2)**, 78 (1999)
16. Wong, L., Ostrander, D., Erb, U., Palumbo, G. and Aust, K.T., *Nanophases and Nanocrystalline Structures*, Edited by R.D. Shull and J.M. Sanchez, TMS, pp. 85-93 (1994)
17. Bonino, J.P., Bruet-Hotellaz, S., Bories, C., Poudroux, P. and Rousset, A., *J. Appl. Electrochem.* **27**, 1193 (1997)
18. Boylan, K., Ostrander, D., Erb, U., Palumbo, G. and Aust, K.T., *Scripta Metall. et Mater.*, **25**, 2711 (1991)
19. Osmola, D., Nolan, P. Erb, U., Palumbo, G. and Aust, K.T., *Phys. Stat. Sol. (a)*, **131**, 569 (1992)
20. Mehta, S.C., Smith, D.A. and Erb, U., *Mat. Sci. Eng.* **A204**, 227 (1995)
21. Rofagha, R., Erb, U., Ostrander, D., Palumbo, G. and Aust, K.T., *Nanostructured Materials*, **2**, 1 (1993)
22. Rofagha, R. and Erb, U., *Defect Structure, Morphology and Properties of Deposits*, H. Merchant ed., TMS, p.245 (1995)
23. Ostrander, D., "A Study on the Production and Mechanical Behavior of Nanocrystalline NiP Electrodeposits", M. Sc. Thesis, Queen's University, Kingston, Ontario, Canada (1993)
24. Cullity, B.D., *Elements of X-ray Diffraction*, Addison-Wesley Publishing Company, p. 284 (1978)
25. Knotek, O., Lugscheider, E., Loffler, F., Kramer, G. and Zimmermann, H., *Surf. Coat. Tech.*, **68/69**, 489 (1994)
26. Maejima, M., Saruwatari, K. and Isawa, K., *Metal Finish.*, **96**, 37 (1998)
27. Massalski, T.B., Murray, J.L., Bennett, L.H. and Baker, H., *Binary Alloy Phase Diagrams*, ASM International, Materials Park, Ohio, p.1739 (1986)
28. Hansen, M. and Anderko, K., *Constitution of Binary Alloys*, McGraw Hill, New York (1958)
29. Bredael, E., Blanpain, B., Celis, J.P. and Roos, J.R., *J. Electrochem. Soc.*, **141**, 294 (1994)
30. Apachitei, I. and Duszczuk, J., *Surf. Coat. Tech.*, **132**, 89 (2000)
31. Chokshi, A.H., Rosen, A., Karch and Gleiter, H., *Scripta Metall. et Mater.*, **23**, 1679 (1989)

32. Palumbo, G., Erb, U. and Aust, K.T., *Scripta Metall. et Mater.*, **24**, 2347 (1990)
33. El-Sherik, A.M., U. Erb, G. Palumbo and K.T. Aust, *Scripta Metall. et Mater.*, **27**, 1185 (1992)
34. Cheung, C., Palumbo, G. and Erb, U., *Scripta Metall. et Mater.*, **31**, 735 (1994)
35. Hall, E.O., *Proc. Phys. Soc. (London)*, **B64**, 747 (1951)
36. Petch, N.J., *J. Iron steel Inst.*, **174**, 25 (1953)
37. Schiotz, J., Vegge, T., Di Tolla, F.D. and Jacobsen, K.W., *Phys. Rev.* **B60**, 11971 (1999)
38. Swygenhoven, H. and Caro, A., *Appl. Phys. Lett.* **71**, 1652 (1997)
39. Archard, J.F., *J. Appl. Phys.*, **24**, 981 (1953)